



HAL
open science

Drying of a Solution in a Meniscus: A Model Coupling the Liquid and the Gas Phases

Frédéric Doumenc, B. Guerrier

► **To cite this version:**

Frédéric Doumenc, B. Guerrier. Drying of a Solution in a Meniscus: A Model Coupling the Liquid and the Gas Phases. *Langmuir*, 2010, 26 (17), pp.13959-13967. 10.1021/la1018373 . hal-04486250

HAL Id: hal-04486250

<https://hal.science/hal-04486250>

Submitted on 1 Mar 2024

HAL is a multi-disciplinary open access archive for the deposit and dissemination of scientific research documents, whether they are published or not. The documents may come from teaching and research institutions in France or abroad, or from public or private research centers.

L'archive ouverte pluridisciplinaire **HAL**, est destinée au dépôt et à la diffusion de documents scientifiques de niveau recherche, publiés ou non, émanant des établissements d'enseignement et de recherche français ou étrangers, des laboratoires publics ou privés.

Drying of a solution in a meniscus: a model coupling the liquid and the gas phases

Doumenc F.* and Guerrier B.

*UPMC Univ Paris 06, Univ Paris-Sud, CNRS, lab. FAST, bat 502, Campus Univ., Orsay F-91405,
France*

E-mail: frederic.doumenc@upmc.fr

Abstract

A model simulating the drying of a solution in a meniscus in contact with a moving substrate is developed. It takes into account the hydrodynamics in the solution in the framework of lubrication approximation, the vapor diffusion in the gas phase and the variation of physical properties during drying. The free surface profile and spatial evaporation flux are not imposed a priori but result from the simulation of the mass transfer in the liquid/gas system (1.5 sided model). Several regimes are observed depending on the substrate velocity. For large substrate velocity the classical Landau-Levich regime is obtained. For smaller velocities a drying front appears which is characterized by a strong concentration gradient and a peak of the evaporation flux. The coupling between the evaporation flux and the meniscus shape in this regime is analyzed. At last another regime appears at very low substrate velocity and seems driven by a competition between advection and diffusion. This macroscopic model simulates recent experimental results, namely the dependence of the deposit thickness on the substrate velocity, which scales as $1/V$ in the regime dominated by evaporation.

*To whom correspondence should be addressed

Introduction

Evaporation in the vicinity of a contact line or in a meniscus has been the focus of numerous experimental and theoretical studies during the last years. Indeed, despite its apparent simplicity, this problem involves complex physics due notably to the coupling between the hydrodynamics in the liquid and the mass transfer in the gas phase. Understanding the dominant phenomena which control the evaporation is also a challenging problem for applications, since many coatings are obtained by drying a solution or a suspension. Numerous recent experimental studies are devoted to the obtention of uniform coatings or structured ones for specific applications.

Boundary effects due to the presence of a contact line or a meniscus, that are encountered for example in droplet drying or dip coating, induce strong spatial variations of the evaporation flux and then a liquid flow. As a consequence the dried deposit may exhibit complex morphology like periodic patterns due to stick/slip phenomena. For instance the famous coffee stain effect studied by Deegan *et al*¹ requires the coupling of the hydrodynamic flow inside the droplet and the ability for the deposit to pin the contact line. Since then several experimental or theoretical works have been developed for different geometries such as droplets, dip coating or similar experiments with a moving substrate. Several types of material have been investigated, such as colloids including silica particles²⁻⁴ and polymer beads,^{5,6} but also small molecules,⁷ carbon nanotubes,⁸ polymers^{9,10} and biological molecules.¹¹ Some characteristics of the deposition process seem to be generic and relatively independent of the nature of the material.¹² Modeling the coupling between the hydrodynamics in the liquid and the transfer in the gas is then an interesting working track to better understand the deposit formation.

In this study we focus on evaporation of a volatile liquid in an inert gas so that evaporation is limited by the diffusion of solvent vapor in the gas. The physical phenomena which control the evaporation kinetics are then different from one fluid systems where the solvent vapor is the only gas, like for instance in heat-pipes.¹³ Several works investigate the flow induced by evaporation in the vicinity of a contact line for a pure volatile liquid evaporating in ambient air. In most of the cases lubrication approximation is used and the spatial variation of the evaporation flux or the

free surface geometry are fixed a priori. Suspensions have also been studied but most often without taking into account the effect of particle concentration on fluid hydrodynamics. The deposit is then only a signature of the flow field obtained for the pure liquid. With these assumptions simulations are performed to get the flow field inside the liquid induced by evaporation and/or Marangoni effect. Depending on the parameters the deposit can be uniform, more important at the external edge of the droplet ("coffee stain" effect) or on the contrary concentrated at the center. For instance Fischer¹⁴ analyzes the influence of different evaporation flux profiles on the particle flow direction (towards the center or the edge) for evaporating droplets without Marangoni effect. Petsi and Burganos¹⁵ also consider a fixed evaporation profile and study the particle flow for pinned or unpinned contact lines, with Stokes 2D equations and Navier slip condition at the contact line. Berteloot et al.¹⁶ develop a model to estimate the meniscus deformation induced by evaporation. The coupling between different evaporation flux profiles and Marangoni flow has been considered by Murisic and Kondic¹⁷ for pure liquid, without pinning. Hu and Larson¹⁸ have compared water and organic solvents for spherical droplets with a given evaporation flux and thermal Marangoni effect. They explain the difference in the dried deposit (deposit at the center or the edge) by annihilation of Marangoni flow in water droplets, due to the surface contamination.

To our knowledge studies taking into account explicitly the dependence of physical properties with the concentration for such geometries are more sparse. Recently Craster and co-authors¹⁹ have developed a model to analyze pinning, retraction and terracing of droplets containing nanoparticles. In the hydrodynamic model the authors take into account the concentration dependence of the viscosity and use a disjoining pressure approach to describe small scale interactions. The evaporation is driven by the departure from equilibrium at the interface. Thiele²⁰ and co-authors develop a similar approach as well as statistical models to characterize contact line pinning or dewetting for evaporating thin films. Numerous references to experimental or numerical works can be found in their review paper. The effect of a strong increase of the viscosity at the contact line has also been analyzed experimentally by Monteux et al.¹⁰ on polymer droplets.

In this paper we use a macroscopic description taking into account the hydrodynamics in the

solution, the variation of physical properties during drying and the coupling with the gas phase (drying in air at atmospheric pressure). The free surface profile and spatial evaporation flux are then not imposed a priori but result from the simulation of the mass transfer in the liquid/gas system. The objective is to show that several experimental results, namely the deposit thickness, can be explained by this quite simple macroscopic model, neglecting physicochemical interactions with the substrate and assuming newtonian rheology. This study follows recent experimental works where different systems (biological molecules, colloidal suspensions and polymer solutions) have been dried on a moving substrate. Geometries are close to dip coating experiments. In the work of Le Berre et al.¹¹ a droplet of phospholipid solution is dragged on a substrate at constant speed. In our previous work a capillary rise is achieved between two glass plates immersed in a reservoir.¹² The position of the capillary rise is governed through the emptying of the reservoir, achieved using a syringe pump. The accessible range of flow rates allows us to explore contact line velocities from less than $1\mu m/s$ up to $2mm/s$. Several regimes have been observed when varying the substrate velocity depending on the capillary number, Ca , that compares capillary to viscous forces, with $Ca = \eta V/\gamma$, η being the dynamic viscosity, V the substrate velocity and γ the surface tension (we consider only small velocities for which inertial effects can be neglected). For sufficient capillary number, viscous forces are large enough to drag a film from the bath. This regime is known as the Landau-Levich regime^{21,22} and the thickness of the dragged film is proportional to $Ca^{2/3}$. The Landau model has been established for the dip coating geometry but can be easily adapted to our confined geometry, where the gap d between the two plates is smaller than the capillary length. Compared to the Landau theory, the only modification concerns the fit between the static and dynamic meniscus. The static curvature to take into account in our case is simply the inverse of the static meniscus radius, equal to $2/d$. This leads to:

$$h = 0.67 d Ca^{2/3} \quad (1)$$

For smaller capillary numbers another regime was observed where the film thickness varies in the opposite way, i.e., it increases when the velocity decreases. The dried thickness is found

proportional to about V^{-1} , whatever the system. Moreover, the following relation was obtained

$$h_d \sim \frac{F \phi_0}{V} \quad (2)$$

where ϕ_0 is the solute volume fraction in the bulk and F the evaporation flux measured with pure liquid (cf. more details in the section dedicated to the evaporation flux). Experimental observations show that this relation holds for systems as different as small molecules, colloidal suspensions or polymer solutions and ask for deeper investigation to understand what are the dominant phenomena involved in this regime. The model developed in this paper describes the way the evaporation flux and concentration profile take shape for different substrate velocities. It explains the different regimes observed experimentally and more generally gives new insight in the coupling between liquid and gas and its consequence on evaporation and meniscus shape.

Problem formulation

Model equations

We consider the drying in a meniscus of a binary solution composed of one volatile solvent and one nonvolatile solute, on a moving flat substrate. The temperature is assumed constant (isothermal problem). Coupled mass transfers in the liquid and in the gas phases are taken into account. Drying takes place in air at atmospheric pressure, local thermodynamic equilibrium is assumed at the interface and the evaporation is limited by the solvent vapor transfer into the air. Complete description of the gas phase dynamics (2-sided model) would be too complex. For sake of simplicity the air is assumed stagnant but diffusive bidimensional effects in the gas are taken into account and turn out to be one of the key aspect controlling the drying behavior, as will be seen in the following. This is the so-called 1.5-sided model which is a compromise between the complete hydrodynamic description and the 1-sided model in which transfer with the surroundings is estimated with an a priori known mass transfer coefficient. At last, it can be shown that in the regime where evapora-

tion is the dominant mechanism the substrate velocity is small enough to neglect entrainment of the gas phase induced by the moving substrate.

In the liquid phase the velocity field is assumed quasi-parallel to the substrate (lubrication approximation) with no-slip at the substrate and zero tangential stress at the free surface. The direction of the flow is noted \vec{x} , the axis normal to the substrate is \vec{z} . Gravity as well as Marangoni effect are neglected. Another important assumption concerns the concentration in the liquid phase which is assumed uniform on the thickness. Indeed taking into account the 2D concentration field in the solution would make the simulation much more complex, especially with a deformable interface. This assumption is consistent with the above description of evaporation limited by the solvent diffusion in the air. In most of the configurations considered in the following, diffusion velocity in the liquid is large enough to ensure a uniform concentration in the \vec{z} direction. This assumption may become questionable in the thick part of the meniscus for the smallest diffusion coefficient tested in this study. Nevertheless in the first step considered in this paper concentration variations in the \vec{z} direction are not taken into account. With the above-mentioned approximations and assuming a newtonian fluid, Stokes equations lead to the standard result:^{23,24}

$$Q(x, t) = \frac{h^3}{3\eta} \frac{\partial}{\partial x} \left(\sigma \frac{\partial^2 h}{\partial x^2} \right) + Vh \quad (3)$$

where h is the liquid height, η the dynamic viscosity, σ the surface tension and V the substrate velocity. $Q(x, t)$ is the liquid volume flux at abscissa x and time t over a cross section normal to \vec{x} (by unit of width),

$$Q(x, t) = \int_0^{h(x)} u(x, z) dz \quad (4)$$

where $u(x, z)$ is the velocity component in the \vec{x} direction.

The global mass conservation and the nonvolatile solute mass conservation read respectively:²⁰

$$\frac{\partial h}{\partial t} + \frac{\partial Q}{\partial x} = -v_{ev}(x,t) \quad (5)$$

$$\frac{\partial(\phi h)}{\partial t} + \frac{\partial(\phi Q)}{\partial x} = \frac{\partial}{\partial x} (h D_{mut} \frac{\partial \phi}{\partial x}) \quad (6)$$

where $v_{ev}(x,t)$ is the local evaporation velocity (positive for evaporation), ϕ the solute volume fraction and D_{mut} the mutual diffusion coefficient of the binary system (Fick law written with the assumption of constant liquid density).

The boundary conditions are the following: At $x = 0$ we assume that we get the bulk solute volume fraction, ϕ_0 , and we impose the liquid height h_0 and the curvature C_0 (Eq. (7)). If one performs an analogy with previous capillary rise experiments,¹² C_0 is the curvature of a static meniscus, deduced from the gap d between the plates: $C_0 = 2/d$, with $d = 1mm$. The lubrication theory is valid if the free surface slope is much lower than 1, which is true if h_0 is small enough. In all the results presented in the following $h_0 = 100\mu m$ (some other calculations were performed with $h_0 = 30\mu m$ and give the same results concerning the deposit thickness or the evaporation flux, so that they are not presented here). Spatial derivatives of h in Eq. (5) and ϕ in Eq. (6) being respectively of fourth and second order, three boundary conditions are also needed at $x = W$. These outlet conditions far from the bulk are given in Eq. (8) (As far as the length of the simulation box is large enough, the choice of the outlet conditions is not very important since they do not modify significantly the upstream flow).

$$\text{at } x = 0 : \quad h = h_0, \quad \frac{\partial^2 h}{\partial x^2} = C_0, \quad \phi = \phi_0 \quad (7)$$

$$\text{at } x = W : \quad \frac{\partial h}{\partial x} = 0, \quad \frac{\partial^2 h}{\partial x^2} = 0, \quad \frac{\partial \phi}{\partial x} = 0 \quad (8)$$

The local evaporation velocity in Eq. (5) is determined by solving a diffusion problem in the gas phase, in a domain of length W and height H , shown in Figure 1 (for process with a forced air flow above the free surface, H would roughly correspond to the boundary layer thickness). Since H

is much larger than h_0 , we assume a rectangular domain for the gas phase. This means that liquid thickness variations are neglected when computing mass transfer in the gas phase. The bottom boundary of this domain corresponding to the liquid-gas interface is then: $z = 0$ and $0 < x < W$. The diffusion equation in the gas phase reads:

$$\frac{\partial c_g}{\partial t} = D_g \left(\frac{\partial^2 c_g}{\partial x^2} + \frac{\partial^2 c_g}{\partial z^2} \right) \quad \text{for } 0 < x < W \quad \text{and} \quad 0 < z < H \quad (9)$$

where c_g is the solvent vapor concentration in the air. The vertical walls are assumed impermeable. At the top a Dirichlet condition is imposed, with solvent vapor concentration equal to 0. Then we get the following boundary conditions for the gas domain:

$$\frac{\partial c_g}{\partial x} = 0 \quad \text{for } (x = 0 \text{ or } x = W) \quad \text{and} \quad 0 < z < H \quad (10)$$

$$c_g = 0 \quad \text{for } 0 \leq x \leq W \quad \text{and} \quad z = H \quad (11)$$

The last boundary condition corresponds to the coupling between the liquid and the gas phases and is achieved by writing the mass flux conservation and the local thermodynamic equilibrium at the interface:

$$\rho v_{ev} = -D_g \frac{\partial c_g}{\partial z} \quad \text{for } 0 \leq x \leq W \quad \text{and} \quad z = 0 \quad (12)$$

$$c_g = a(\phi, T) P_{vs0}(T) \frac{M_s}{RT} \quad \text{for } 0 \leq x \leq W \quad \text{and} \quad z = 0 \quad (13)$$

where ρ is the liquid solvent density, M_s the solvent molar mass, R the ideal gas constant, T the temperature, P_{vs0} the saturated vapor pressure of the pure solvent, and a the activity of the solvent at the interface (with the assumption that the solvent vapor behaves like an ideal gas, its activity is the ratio of the partial vapor pressure over the saturated vapor pressure of the pure solvent). The effect of the capillary pressure on the solvent chemical potential is neglected. As already said, evaporation cooling effect is disregarded so the temperature T is assumed uniform in the whole system, and equal to the room temperature.

This paper mainly focuses on the steady state and we use as initial conditions the result of a previous calculus for a close configuration. It has been checked that the choice of the initial conditions has no effect on the steady state result.

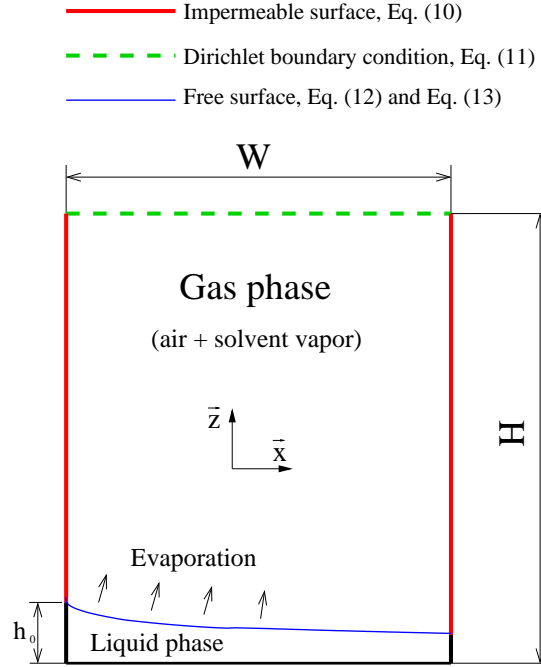


Figure 1: Sketch of the problem geometry

The above set of equations (Eq. (3) to Eq. (13)) is solved numerically by finite differences, using a pure implicit scheme of order 1 in time and 2 in space. At each time step, equations are solved iteratively in the liquid and in the gas, until convergence is achieved. The discretization of equations in the liquid (Eq. (3) to Eq. (8) and Eq. (12)) leads to a set of nonlinear algebraic equations, solved by Newton-Raphson algorithm. An adaptive mesh is implemented, in order to refine the mesh in region of high concentration gradient. In the gas phase, the set of algebraic equations resulting from discretization of equations Eq. (9) to Eq. (11) and Eq. (13) is linear, and solved by Successive Over-Relaxation method (SOR). A specific software has been written in Fortran, and most of the computations have been performed on iDataPlex IBM clusters. Computational time vary from a few minutes in the Landau-Levich regime, to several weeks in the evaporative regime.

The solution gives the meniscus shape, the local evaporation flux and the concentration field in the gas, as well as the concentration and velocity fields in the solution as a function of the control

parameters (substrate velocity, bulk solute concentration, solution properties and geometry).

In this model microscopic-scale interactions with the substrate are not taken into account. No limitation is a priori imposed on the thickness $h(x)$ that can become close to zero. In that case the above equations are no more valid and other model, introducing for instance a disjoining pressure, should be used. Nevertheless the aim of this paper is to show that a simple model coupling transfer in the gas and in the solution can explain some of the observed experimental behaviors. When the thickness goes to zero for some values of the control parameters, the above model does not intend to give a physical description of the film but points out a change in the drying regime.

Data

Geometric characteristics are the following. For all computations we have $W = 1mm$, $h_0 = 0.1mm$, $C_0 = 2mm^{-1}$. Three values have been compared for the box height H : $H = 0.3, 3$ or $30mm$. The bulk solute volume fraction is $\phi_0 = 0.01, 0.05$ or 0.1 . To avoid adjustable parameters we have used a model system whose characterization has been carefully performed in previous studies, that is a Polyisobutylene/toluene solution. All the simulations are done at $T = 25^\circ C$. Variations of the density ρ and surface tension σ with the solvent concentration are neglected and we use the following values: $\rho = 900kg.m^{-3}$, $\sigma = 30mN.m^{-1}$. Toluene saturated vapor pressure, molar mass and diffusion coefficient in the gas phase are, respectively: $P_{vs0} = 3792Pa$, $M_s = 92.14g.mol^{-1}$ and $D_g = 8.6 \times 10^{-6}m^2.s^{-1}$.

For polymer solution, it is well known that the solution viscosity strongly depends on the polymer molar mass and polymer concentration. Except when specified, the viscosity used in the simulations corresponds to a molar mass $M_W = 500 kg.mol^{-1}$. Some simulations were also made with the viscosity corresponding to a larger molar mass $M_W = 10^3 kg.mol^{-1}$. To express the dependence on polymer concentration the following empirical fit^{25,26} have been used (Figure 2):

$$y = 8.22 + 13.2 x + 5.2 x^2 + 0.70 x^3 \quad \text{for } M_W = 500 kg.mol^{-1} \quad (14)$$

$$y = 9.26 + 11.94 x + 3.86 x^2 + 0.42 x^3 \quad \text{for } M_w = 10^3 \text{ kg.mol}^{-1} \quad (15)$$

with $y = \log_{10}(\eta)$ and $x = \log_{10}(\phi)$.

The concentration dependence of the activity and mutual diffusion coefficient have been obtained from gravimetry experiments.²⁷ The activity depends on polymer concentration and is given by the Flory-Huggins law, plotted in Figure 3(a):

$$a(\phi) = (1 - \phi) \exp(\phi + \chi \phi^2) \quad \text{with } \chi = 0.45 + 0.30\phi \quad (16)$$

For the mutual diffusion coefficient D_{mut} , the following constant values have been considered: $D_{mut} = 10^{-11}, 10^{-10}, 10^{-9} \text{ m}^2 \cdot \text{s}^{-1}$, and also a concentration dependent function given by:²⁷ (Figure 3(b)):

$$\log_{10}(D_{mut}) = -9.85 - 0.14 \phi + 0.78 \phi^2 + 3.61 \phi^3 - 7.39 \phi^4 \quad (17)$$

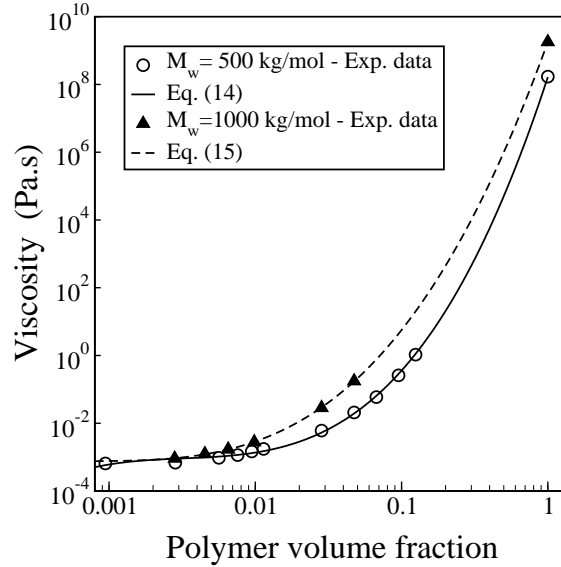


Figure 2: viscosity of PIB/Toluene solutions for two molar masses.

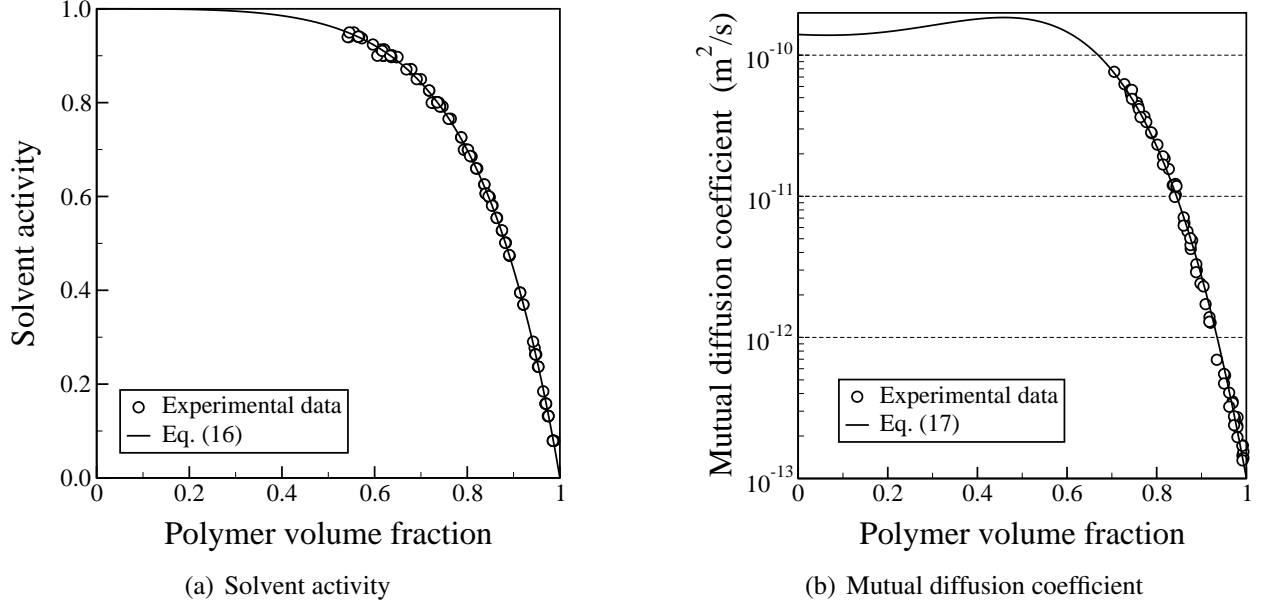


Figure 3: Thermodynamic characteristics of PIB/Toluene solutions. The experimental points have been obtained in the concentrated domain. The mutual diffusion coefficient fit is then extended to the dilute domain where D_{mut} is of the order of $10^{-10} m^2 s^{-1}$ and where no important variation of D_{mut} is expected.

Local description - meniscus shape, concentration and velocity fields

We first analyze the coupling between the evaporation and hydrodynamics for the following configuration: $\phi_0 = 0.01$, $M_w = 500 kg.mol^{-1}$, $H = 3mm$, $D_{mut} = 10^{-10} m^2/s$. The substrate velocity is varied on two orders of magnitude, $10 \mu m.s^{-1} \leq V \leq 1 mm.s^{-1}$. Then the capillary number $Ca = \eta V / \sigma$ that compares capillary to viscous forces ranges from 4.5×10^{-7} to 4.5×10^{-5} .

The corresponding meniscus shape, local polymer volume fraction, evaporation flux and liquid velocity are given in Figure 4. Meniscus shape is plotted in semilog-scale to get a better view of the meniscus profile.

At the largest substrate velocity ($V = 1 mm.s^{-1}$ and $Ca = 4.5 \times 10^{-5}$), a film of about $1 \mu m$ is pulled out from the bath, due to viscous forces (dark blue curve in Figure 4(a)). This corresponds to the well known Landau-Levich regime described in dip coating experiments and will be discussed in next section. In this regime of high substrate velocity, evaporation has no significant effect.

Indeed the evaporation flux is uniform on the whole film length and too small for the polymer concentration to change much when the solution flows from $x = 0$ to $x = W$. As a consequence, the concentration field in the gas phase is quasi one-dimensional (Figure 5(a)).

When decreasing the substrate velocity, a drying front appears which is characterized by a strong concentration gradient and a peak of the evaporation flux (Figure 4(a)-(c)). The concentration field in the gas phase is now two-dimensional as shown in Figure 5(b). Diffusion in the \vec{x} direction induces a curvature of the concentration isolines, so that the vapor concentration gradient above the surface in the \vec{z} direction is very small at the right of the evaporation peak. As a consequence the evaporation flux falls down and becomes very weak (Figure 4(c)), while the activity is still larger than 0.5. In this regime, called evaporative regime in the following, evaporation and hydrodynamics are strongly coupled. Let us note that we recover the tip effect described by Deegan and co-authors¹ in the analysis of the coffee stain effect. But here we have no flux divergence because the liquid considered in the model is a binary solution including a non volatile component, so the film thickness doesn't vanish anywhere, and we get a continuous (even if steep) concentration field (a very refined mesh is used in the front zone to capture accurately the evaporation peak shape).

Another important result concerns the meniscus structure. For all the substrate velocities, one can observe that the last part is "frozen" (i.e. the liquid velocity is equal to the substrate velocity) while a flow in the substrate frame is observed in the first part of the box, due to the substrate movement and evaporation (Figure 4(d)). As detailed below, simulation results show a strong correlation between the meniscus shape, the evaporation flux and the liquid velocity in the evaporative regime. The meniscus height and its spatial derivative (slope) are displayed in Figure 6(a) and Figure 6(b) for $V = 30\mu s^{-1}$. The spatial evolution of the slope reveals that the meniscus can be divided into two parts. In the first one the linear variation of the slope implies a constant curvature, equal to the curvature imposed at the boundary condition at $x = 0$. This part will be called "quasi-static meniscus" since friction is not strong enough to modify the curvature significantly (red dotted lines in Figure 6(a) and Figure 6(b)). Then a steep transition occurs where the slope derivative

(meniscus curvature) suddenly changes. In the second part of the meniscus the slope goes to zero on a length of a few microns. We can also see on Figure 6(b) that the transition between the two zones corresponds to the maximum of the evaporation flux on one hand (vertical dotted line) and to the transition between the "flowing" and "frozen" zone on the other hand. Indeed the transition between these two zones occurs when $u = V$ and can be clearly displayed by superimposing the simulated profile and the one obtained by stating $u = V$ in the mass balance steady state equations (from Eq. (4) and Eq. (5)):

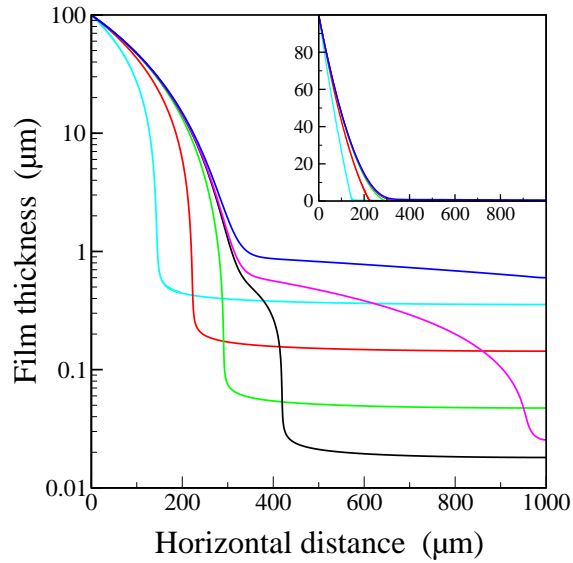
$$\frac{\partial h}{\partial x} = -\frac{v_{ev}(x)}{V} \quad (18)$$

where $v_{ev}(x)$ is the evaporation velocity obtained from the simulation (cf. blue dashed line in Figure 6(a) and Figure 6(b)). These three phenomena occurring at the same location (steep change in the meniscus curvature, cancelation of the liquid flow and maximum of the evaporation flux) are due to the increase of the polymer concentration. Indeed this induces a large increase of the solution viscosity which annihilates the flow and makes the Laplace pressure unable to maintain the quasi-constant curvature in the meniscus. In addition the meniscus being no more supplied in solvent after the transition, the activity decreases and so does the evaporation flux. Finally the evaporation flux becomes close to zero and after the meniscus we get a quasi-flat film (Eq. (18)). It will be interesting, but beyond the scope of the present paper, to analyze in which configurations these mechanisms hold when taking into account microscopic interactions with the substrate through a disjoining pressure term.

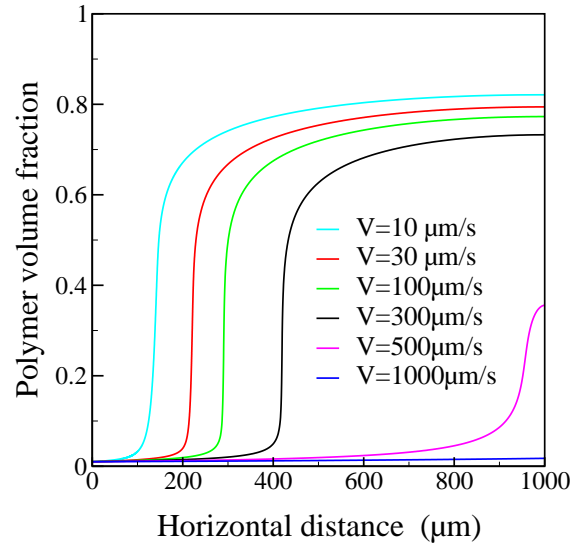
Effect of viscosity and bulk concentration

The consequence of these different regimes on the dried deposit thickness is now analyzed. The final thickness of the dried deposit is obtained by the relation $h_d = \phi(x)h(x)$ where ϕ and h are taken in any point of the "frozen" zone.

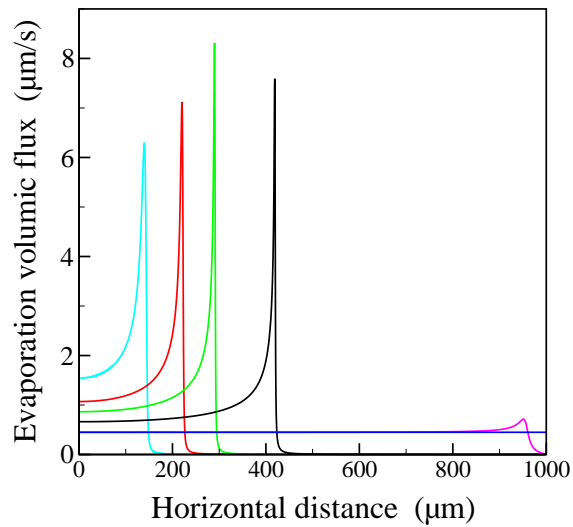
Let us first look at the results obtained with the configuration of the previous section, corresponding to the red circles in Figure 7. As already noticed, several regimes can be observed de-



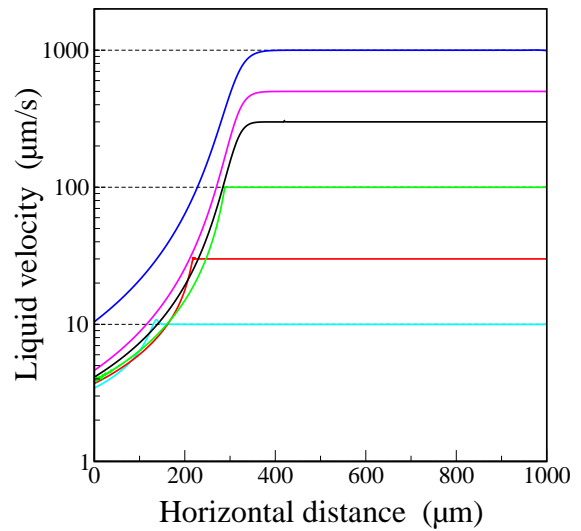
(a) Liquid height



(b) Polymer volume fraction

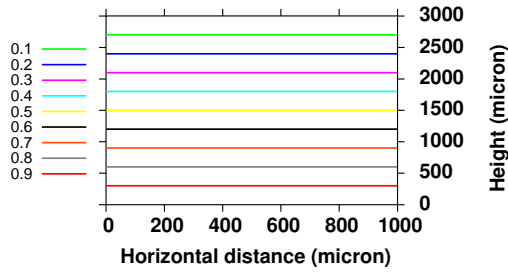


(c) Evaporation flux

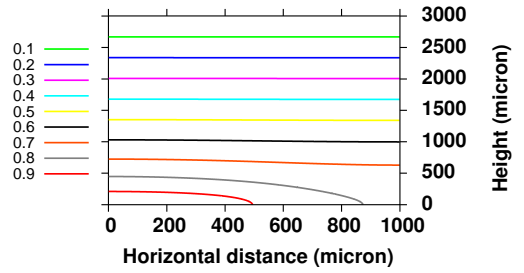


(d) Liquid velocity averaged on a vertical section

Figure 4: Profiles as a function of horizontal distance x for $\phi_0 = 0.01$, $M_w = 500 \text{ kg} \cdot \text{mol}^{-1}$, $H = 3 \text{ mm}$, $D_{mut} = 10^{-10} \text{ m}^2 \cdot \text{s}^{-1}$ and for different substrate velocities. The correspondence between color and substrate velocity is given in Figure 4(b).

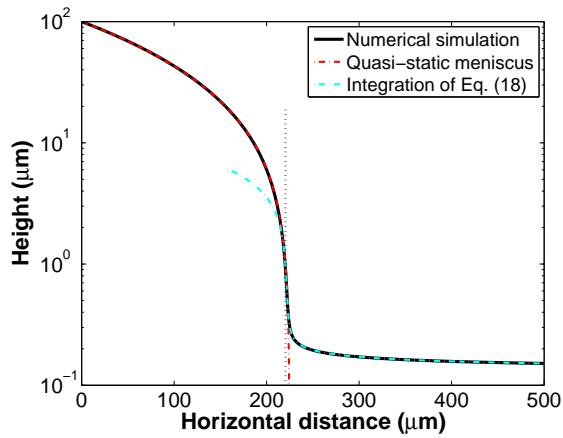


(a) $V = 1000 \mu\text{m}\cdot\text{s}^{-1}$

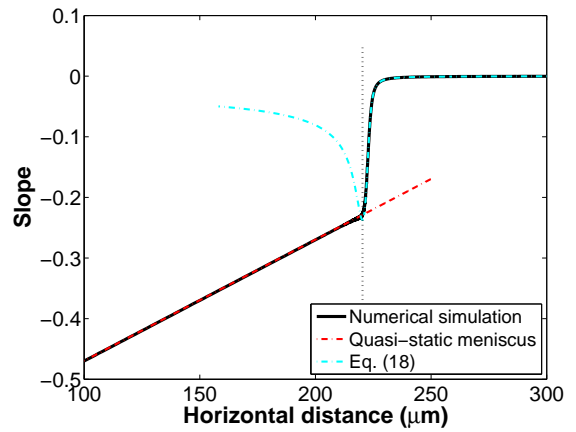


(b) $V = 300 \mu\text{m}\cdot\text{s}^{-1}$

Figure 5: Isovalues of the solvent activity in the gas phase for two substrate velocities V , same conditions than in Figure 4.



(a) Meniscus height



(b) Meniscus slope

Figure 6: Meniscus structure. $V = 30 \mu\text{m}\cdot\text{s}^{-1}$, other parameters are the same than in Figure 4. The vertical black dotted line indicates the position of the maximum of the evaporation flux

pending on the substrate velocity or Capillary number. At high Ca viscous forces prevail, the thickness increases with the substrate velocity. This dynamical wetting regime has been described by Landau and Levich^{21,22} and simulations are in agreement with the thickness deduced from Landau-Levich model, as shown in Figure 7(a) where Eq. (1) is drawn in full line with the viscosity corresponding to the bulk concentration ϕ_0 . But for $V \sim 500\mu m.s^{-1}$ (i.e. $Ca \sim 2 \times 10^{-5}$) a minimum is obtained and the slope of the thickness variation switches to negative value. The dried thickness is proportional to $1/V$ in this regime where evaporation plays a dominant part. This dependence in $1/V$ has been observed experimentally for various systems, like biological molecules¹¹ or colloid suspensions and polymer solutions.¹² At last for very low velocities ($V < 10\mu m.s^{-1}$ for this configuration) another transition appears and the film thickness goes to zero and no steady state can be reached in the framework of this model (in all the curves of Figure 7 the last point on the left corresponds to the smallest velocity that can be handle by the model; below this critical velocity the film thickness goes to zero).

If the viscosity is changed, either by changing the polymer molar mass or by changing the bulk concentration, a strong effect is obtained in the Landau-Levich regime, as expected. The transition from the Landau-Levich regime to the evaporative regime is shifted to lower velocities when the viscosity increases (cf. Figure 7(a)). But scaling the dried thickness by the bulk concentration (h_d/ϕ_0) gathers all the points on the same master curve in the evaporative regime, as shown in Figure 7(b). The viscosity has thus no influence in this regime. This result is consistent with previous experimental observations. Indeed the same scaled dried thickness h_d/ϕ_0 was obtained for polymer solutions with different molar masses or different bulk concentrations.¹²

Evaporation flux and deposit thickness

To study the influence of the box height and then of the evaporation flux, we first analyze the coupling between the meniscus shape and the local evaporation flux in the evaporative regime. Comparison is made with the evaporation of pure solvent. With the geometric assumptions of the

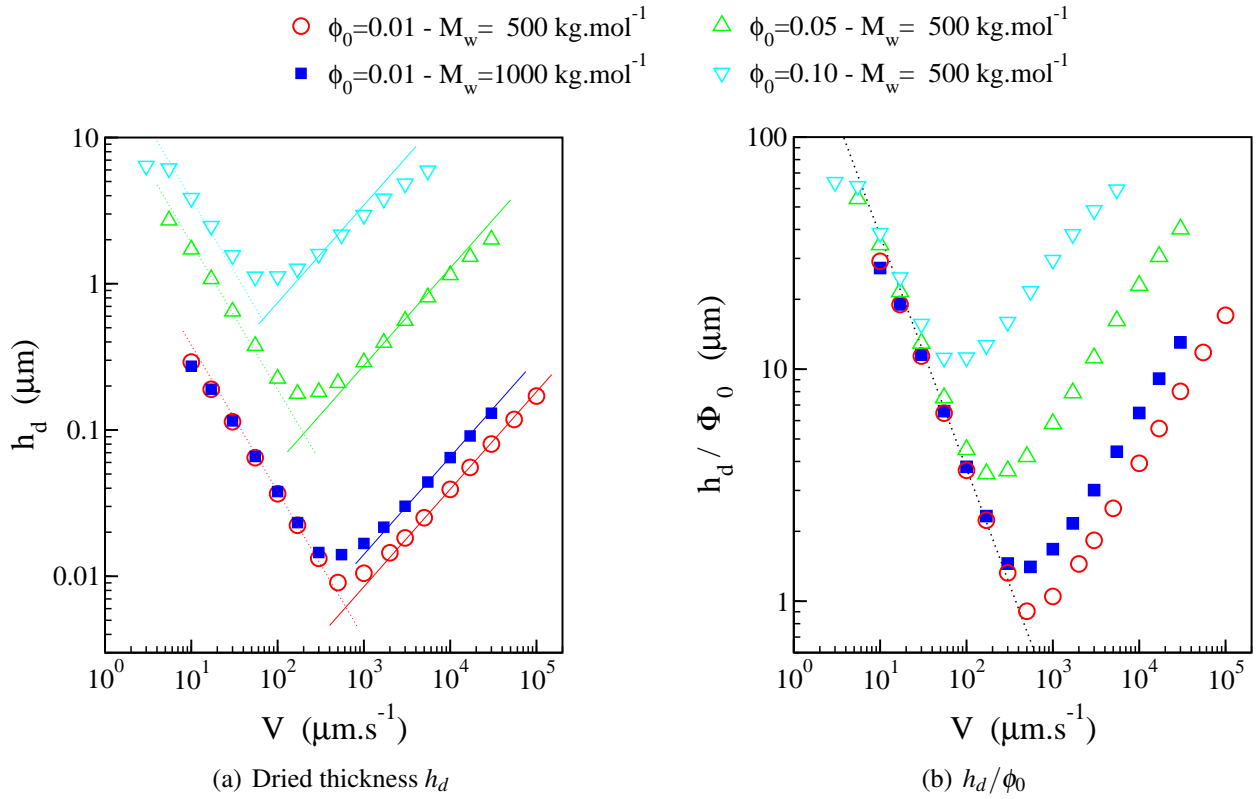


Figure 7: Deposit thickness for different bulk concentrations ϕ_0 and molar masses M_w . $H = 3\text{mm}$, $D_{mut} = 10^{-10}\text{m}^2\text{s}^{-1}$ - Full lines: Landau-Levich model, Eq. (1). Dotted lines: fit with power law V^{-1} .

model, we consider a parabolic meniscus (constant curvature and small slope approximation), of height h_0 at $x = 0$, curvature C_0 , which intercept the substrate at $x = L_{st}$ with 0 contact angle. From this definition we get $L_{st} = \sqrt{2h_0/C_0} \approx 0.316mm$. The local evaporation velocity $v_{ev}^{st}(x)$ is obtained from numerical resolution of the diffusion equation in the gas phase (Eq. (9) to Eq. (11)) with the following boundary conditions at the bottom of the box: evaporation of pure solvent for $0 \leq x \leq L_{st}$ ($a(\phi, T) = 1$) and impermeability for $L_{st} \leq x \leq W$. The mean evaporation velocity \bar{v}_{ev}^{st} and the total flux for the pure solvent F_{ev}^{st} are then

$$F_{ev}^{st} = \int_0^{L_{st}} v_{ev}(x) dx, \quad \bar{v}_{ev}^{st} = \frac{F_{ev}^{st}}{L_{st}} \quad (19)$$

They are given for three values of the box height H in Table 1.

Table 1: Pure solvent evaporation rate as a function of gas domain height H

H (mm)	\bar{v}_{ev}^{st} ($\mu m \cdot s^{-1}$)	F_{ev}^{st} ($\mu m^2 \cdot s^{-1}$)
30	0.14	45
3	1.2	3.9×10^2
0.3	6.4	2.0×10^3

Let L_{ev} be the length corresponding to significant evaporation for the solution on the moving substrate (L_{ev} can also be considered as an estimation of the meniscus size as seen in the section dedicated to the meniscus structure). For example it can be defined as the length where the evaporation flux is larger than 3% of the maximal value of the evaporation peak for a given configuration (cf. for instance Figure 4(c)). The mean evaporation rate \bar{v}_{ev} and total evaporation flux F_{ev} are then defined in the following way:

$$F_{ev} = \int_0^W v_{ev}(x) dx, \quad \bar{v}_{ev} = \frac{F_{ev}}{L_{ev}} \quad (20)$$

For the intermediate value of H ($H = 3mm$, $F_{ev}^{st} = 3.9 \times 10^2 \mu m^2 \cdot s^{-1}$), changing the substrate velocity or the system characteristics leads to large changes of L_{ev} as shown in Figure 8(a). Large variations of the global evaporation flux F_{ev} could then be expected. In fact this is not the case as the mean evaporation rate \bar{v}_{ev} varies in the opposite way, as illustrated in Figure 8(b). The two

effects compensate each other and the ratio F_{ev}/F_{ev}^{st} is close to one whatever the substrate velocity and system properties (cf. Figure 8(c)).

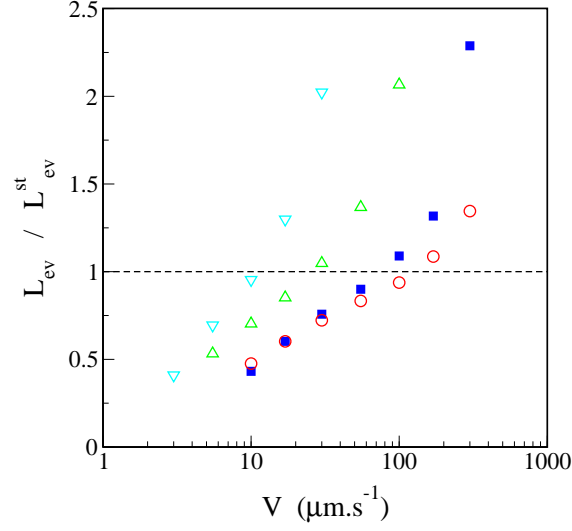
For $H = 30mm$ (i.e. a smaller value of $F_{ev}^{st} = 45 \mu m^2.s^{-1}$), the ratio F_{ev}/F_{ev}^{st} is also close to one (cf. blue symbols in Figure 9(c)). It is only for the smallest value of H ($H = 0.3mm$, $F_{ev}^{st} = 2.0 \cdot 10^3 \mu m^2.s^{-1}$), that this result does not hold any more (cf. green symbols in Figure 9(c)). Indeed, if L_{ev} is much larger than H , the vapor diffusion between the evaporative part of the free surface and the top of the box is mainly 1D, since 2D effects at the end of the evaporative zone can be neglected. As a consequence, in that case, F_{ev} should be proportional to L_{ev} . Here $H = 0.3mm$ is of the same order than L_{ev} so that the concentration field in the gas is between the 2D and 1D regimes.

The effect of the global evaporation flux on the deposit thickness is illustrated in Figure 9(b). As expected the Landau-Levich regime is unchanged while the evaporative regime is strongly dependent of F_{ev} . Moreover the points corresponding to $H = 0.3mm$, and then to a non constant F_{ev} , do not follow a decrease in $1/V$. But scaling the dried thickness by F_{ev} gathers all the points on the master curve $1/V$ in the evaporative regime (Figure 9(c)), so that we get the following expression in this regime:

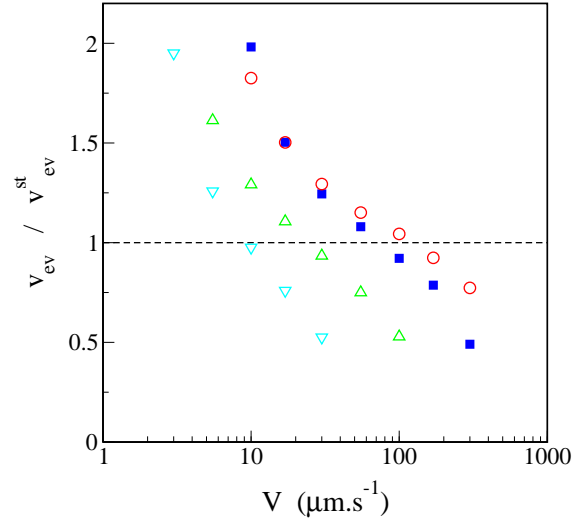
$$h_d = \frac{F_{ev} \times \phi_0}{V} \quad (21)$$

Eq. (21) is similar to the expression used in the paper of Le Berre et al.¹¹ and in our previous experimental work,¹² where it was deduced from a simple approach based on global mass balances. This relation between the thickness, the evaporation flux and the substrate velocity is then characteristic of the steady evaporative regime, for geometries where the meniscus is in contact with an infinite reservoir (then it is not valid for droplets). This simple model assumes that all the solute that enters in the evaporative zone contributes to the dried film. This would be wrong in the case of non negligible concentration gradient in the thickness (not taken into account in our simulations). In that case, recirculation flow would induce a solute net flux towards the bulk, resulting in a distortion of the mass conservation in a section of the meniscus.

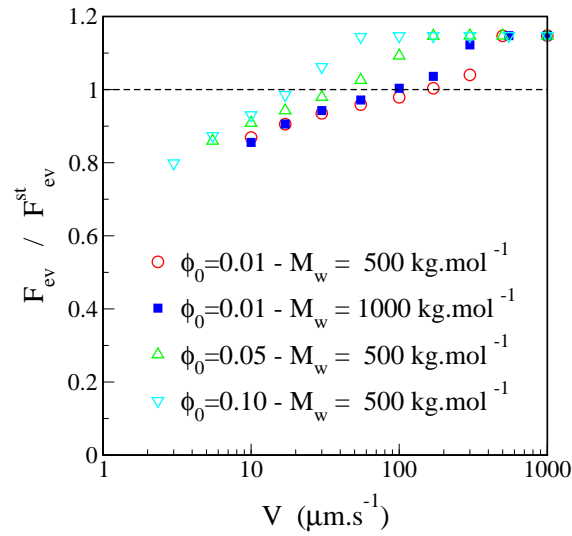
On a practical point of view, the global evaporation flux F_{ev} is however hardly reachable exper-



(a) Evaporation length L_{ev}/L_{ev}^{st}

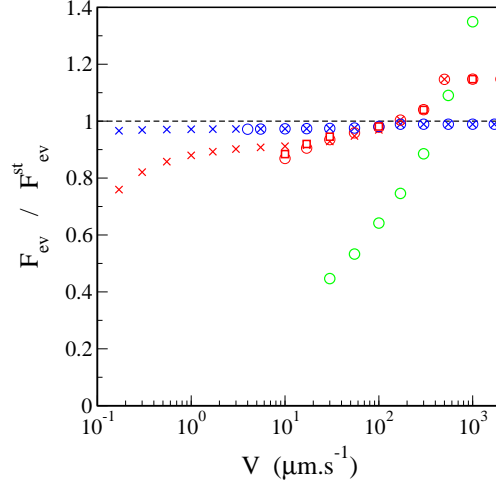


(b) Evaporation velocity v_{ev}/v_{ev}^{st}

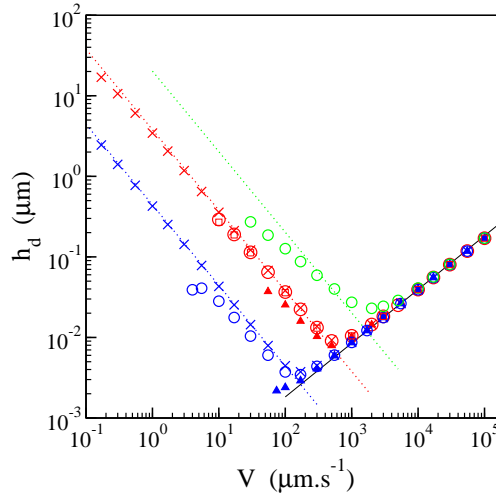


(c) Evaporation flux F_{ev}/F_{ev}^{st}

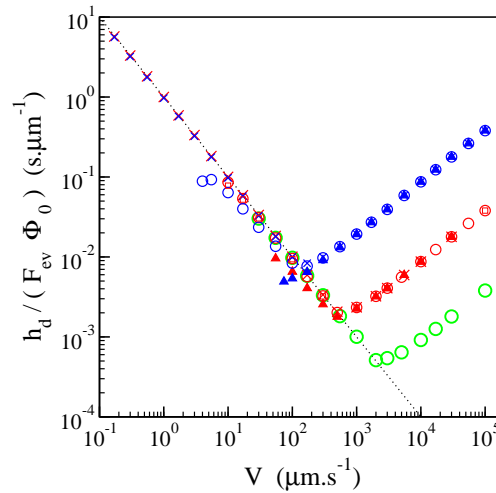
Figure 8: Evaporation length, velocity and flux for different bulk polymer volume fraction ϕ_0 . $H = 3\text{mm}$, $D_{mut} = 10^{-10}\text{m}^2\text{s}^{-1}$ - Same symbols as in Figure 7.



(a) Evaporation flux F_{ev}/F_{ev}^{st}



(b) Dried thickness h_d



(c) $h_d/(F_{ev} \times \phi_0)$

Figure 9: Evaporation flux and dried thickness for different box size and mutual diffusion coefficient. $\phi_0 = 0.01$, $M_W = 500 \text{ kg.mol}^{-1}$ - Box size: $H = 30\text{mm}$ (blue symbols), 3mm (red symbols), 0.3mm (green symbols) - Diffusion coefficient: $2D_{mut} = 10^{-11} \text{ m}^2 \text{ s}^{-1}$ (cross), $10^{-10} \text{ m}^2 \text{ s}^{-1}$ (circle), $10^{-9} \text{ m}^2 \text{ s}^{-1}$ (up triangles), variable D_{mut} (cf. Eq. (17), squares). Dotted lines: fit with power law V^{-1} .

imentally. But as shown above F_{ev} and F_{ev}^{st} are close, provided that H is much larger than L_{ev} , and F_{ev}^{st} can be more easily obtained. This was done in our preliminary experiments¹² by evaporating pure solvent. Even if the geometry of the experimental set-up is not exactly the same as the one simulated here, the same result was obtained, i.e. scaling the experimental thickness by F_{ev}^{st} gathers all the points on the same curve in the evaporative regime.

Mutual diffusion coefficient

The last parameter we have studied is the mutual diffusion coefficient D_{mut} . This coefficient has little effect on the value of the dried deposit thickness, but changes the critical velocity where the evaporative regime stops and the thickness goes to zero (cf. Figure 9(c) and Table 2). The results given in Table 2 have been obtained with $\phi_0 = 0.01$ and $M_w = 500kg.mol^{-1}$, and complementary simulations have shown a weak sensitivity to large change in the viscosity. For each configuration the critical velocity lies between the two values given in the table (a stationary regime was obtained for the largest velocity but not for the smallest one). The symbol $<$ means that the end of the evaporative regime was not observed in the explored domain of velocities.

Hence It seems that the diffusion plays a dominant part in the transition and that it is induced by the development of a polymer counter flux, due to diffusion, from the meniscus to the bulk. These are preliminary results since, as said before, the simulation of this regime should need a modification of the model used here. It will then be interesting to investigate this diffusive flux as a possible mechanism responsible for deposit patterning.

Table 2: End of the evaporative regime - critical velocity in $\mu m.s^{-1}$ ($\phi_0 = 0.01$, $M_w = 500kg.mol^{-1}$).

$D_{mut} (m^2.s^{-1})$	$H = 30mm$	$H = 3mm$	$H = 0.3mm$
10^{-9}	55-74	30-55	
10^{-10}	3-4	5.5-10	17-30
10^{-11}	< 0.1	< 0.1	
variable (Eq. (17))		5.5-10	

Conclusion

In this paper a macroscopic model of the drying of a binary solution on a moving substrate has been developed for the meniscus. The model takes into account the hydrodynamics in the solution in the framework of lubrication approximation, the vapor diffusion in the gas phase and the variation of physical properties during drying. The free surface profile and spatial evaporation flux are not imposed a priori but result from the simulation of the mass transfer in the liquid/gas system. Several regimes have been observed as a function of the substrate velocity. For large substrate velocity the classical Landau-Levich regime is obtained. For smaller velocities a drying front appears which is characterized by a strong concentration gradient and a peak of the evaporation flux. As a consequence the meniscus can be divided into two parts. In the first one the curvature is quasi-constant and the meniscus can be considered as quasi-static. Then a steep transition occurs corresponding to the maximum of the evaporation flux and to a strong decrease of the liquid flow. In the second part (high viscosity, no flow) the meniscus is shaped by the evaporation flux, which results of the coupling between the liquid and gas phases. It is the viscosification of the meniscus edge that is responsible for the change of the meniscus length when the substrate velocity is varied.

It was also shown that this macroscopic model simulates in a very satisfactory way recent experimental results, namely the dependence of the deposit thickness on the substrate velocity, which varies as $V^{2/3}$ in the Landau-Levich regime and V^{-1} in the regime dominated by evaporation. The model also accounts for the experimental scalings obtained by dividing the thickness by the bulk concentration and evaporation flux. At last another regime appears at very low substrate velocity and seems to be due to a competition between advection and diffusion. Further developments are needed to analyze it. More generally the next step is to complete this model that couples the liquid and gas phases by taking into account small scale interactions between the substrate and the film. Another development would concern the extension of the model to a complete two dimensional simulation.

Acknowledgement

This work was supported by the European Union via the FP7 Marie Curie scheme (grant PITN-GA-2008-214919 (MULTIFLOW)). The numerical calculations have been performed on the computers of the "Direction des Services d'Information, Service Calcul" of the University Pierre et Marie Curie-Paris 6.

References

- (1) Deegan, R. D.; Bakajin, O.; Dupont, T. F.; Huber, G.; Nagel, S. R.; Witten, T. A. *Nature* **1997**, *389*, 827–829.
- (2) Rio, E.; Daerr, A.; Lequeux, F.; Limat, L. *Langmuir* **2006**, *22*, 3186–3191.
- (3) Bodiguel, H.; Doumenc, F.; Guerrier, B. *Eur. Phys. J. ST* **2009**, *166*, 29–32.
- (4) Bodiguel, H.; Doumenc, F.; Guerrier, B. *Langmuir* **2010**, *26*, 10758–10763.
- (5) Abkarian, M.; Nunes, J.; Stone, H. A. *J. Am. Chem. Soc.* **2004**, *126*, 5978–5979.
- (6) Ray, M. A.; Kim, H.; Jia, L. *Langmuir* **2005**, *21*, 4786–4789.
- (7) Xu, J.; Xia, J. F.; Hong, S. W.; Lin, Z. Q.; Qiu, F.; Yang, Y. L. *Phys. Rev. Lett.* **2006**, *96*, 066104.
- (8) Small, W. R.; Walton, C. D.; Loos, J.; Panhuis, M. I. H. *J. Phys. Chem. B* **2006**, *110*, 13029–13036.
- (9) Byun, M.; Hong, S. W.; Zhu, L.; Lin, Z. Q. *Langmuir* **2008**, *24*, 3525–3531.
- (10) Monteux, C.; Elmaalem, Y.; Narita, T.; Lequeux, F. *Epl* **2008**, *83*, 34005.
- (11) Le-Berre, M.; Chen, Y.; Baigl, D. *Langmuir* **2009**, *25*, 2554–2557.
- (12) Jing, G.; Bodiguel, H.; Doumenc, F.; Sultan, E.; Guerrier, B. *Langmuir* **2010**, *26*, 2288–2293.

- (13) Rednikov, A.; Colinet, P. *Microgravity Science and Technology* **2010**, *10.1007/s12217-010-9177-x*, .
- (14) Fischer, B. J. *Langmuir* **2002**, *18*, 60–67.
- (15) Petsi, A. J.; Burganos, V. N. *Phys. Rev. E* **2008**, *78*, 036324.
- (16) Berteloot, G.; Pham, C. T.; Daerr, A.; Lequeux, F.; Limat, L. *Epl* **2008**, *83*, 14003.
- (17) Murisic, N.; Kondic, L. *Phys. Rev. E* **2008**, *78*, .
- (18) Hu, H.; Larson, R. G. *J. Phys. Chem. B* **2006**, *110*, 7090–7094.
- (19) Craster, R. V.; Matar, O. K.; Sefiane, K. *Langmuir* **2009**, *25*, 3601–3609.
- (20) Thiele, U.; Vancea, I.; Archer, A. J.; Robbins, M. J.; Frastia, L.; Stannard, A.; Pauliac-Vaujour, E.; Martin, C. P.; Blunt, M. O.; Moriarty, P. J. *J. Phys.: Condens. Matter* **2009**, *21*, 264016.
- (21) Landau, L.; Levich, B. *Acta Physicochem. USSR* **1942**, *17*, 42–54.
- (22) Quéré, D.; de Ryck, A. *Ann. Phys. Fr.* **1998**, *23*, 1–149.
- (23) Guyon, E.; Hulin, J. P.; Petit, L. *Hydrodynamique physique*; CNRS Editions, 2001.
- (24) Oron, A.; Davis, S.; Bankoff, S. *Rev. Mod. Phys.* **1997**, *69*, 931–980.
- (25) Mark, J. E. *Polymer Data Handbook*; Oxford University Press, 1999.
- (26) Gorand, Y.; Doumenc, F.; Guerrier, B.; Allain, C. *Rhéologie* **2003**, *3*, 22–29.
- (27) Doumenc, F.; Guerrier, B.; Allain, C. *Journal of Chemical and Engineering Data* **2005**, *50*, 983–988.

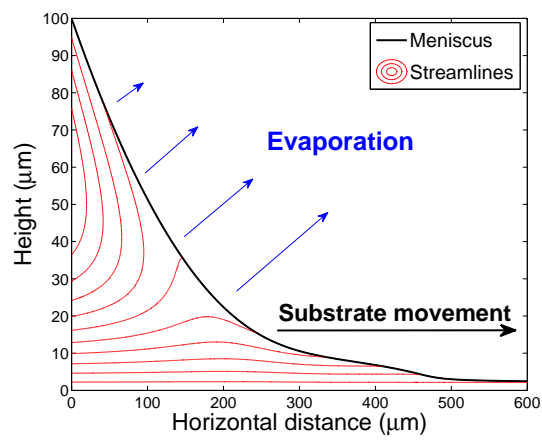
For table of Contents Use Only

Journal: Langmuir

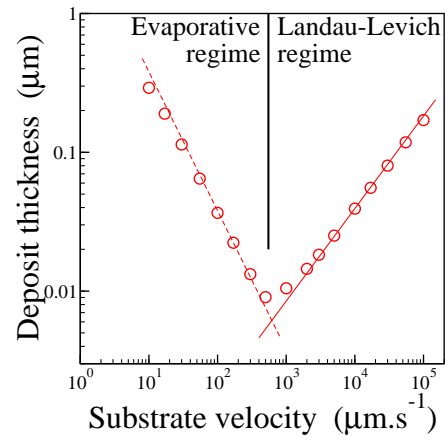
Manuscript ID: la-2010-018373

Title: "Drying of a solution in a meniscus: a model coupling the liquid and the gas phases"

Author(s): Doumenc, Frédéric; Guerrier, Béatrice



(a)



(b)